Chin. Phys. B **33**, 077406 (2024)

SPECIAL TOPIC — Recent progress on kagome metals and superconductors

Two-fold symmetry of the in-plane resistance in kagome superconductor $Cs(V_{1-x}Ta_x)_3Sb_5$ with enhanced superconductivity

Zhen Zhao(赵振)[1,2,†], Ruwen Wang(王汝文)[1,2,†], Yuhang Zhang(张宇航)[1,2], Ke Zhu(祝轲)[1,2], Weiqi Yu(余维琪)[1], Yechao Han(韩烨超)[2], Jiali Liu(刘家利)[1,2], Guojing Hu(胡国静)[1], Hui Guo(郭辉)[1,2], Xiao Lin(林晓)[2], Xiaoli Dong(董晓莉)[1,2], Hui Chen(陈辉)[1,2], Haitao Yang(杨海涛)[1,2,3,‡], and Hong-Jun Gao(高鸿钧)[1,2,3]

[1] *Beijing National Center for Condensed Matter Physics and Institute of Physics, Chinese Academy of Sciences, Beijing 100190, China*
[2] *School of Physical Sciences, University of Chinese Academy of Sciences, Beijing 100049, China*
[3] *Songshan Lake Materials Laboratory, Dongguan 523808, China*

(Received 22 April 2024; revised manuscript received 17 May 2024; accepted manuscript online 24 May 2024)

The kagome superconductor CsV_3Sb_5 has attracted widespread attention due to its rich correlated electron states including superconductivity, charge density wave (CDW), nematicity, and pair density wave. Notably, the modulation of the intertwined electronic orders by the chemical doping is significant to illuminate the cooperation/competition between multiple phases in kagome superconductors. In this study, we have synthesized a series of tantalum-substituted $Cs(V_{1-x}Ta_x)_3Sb_5$ by a modified self-flux method. Electrical transport measurements reveal that CDW is suppressed gradually and becomes undetectable as the doping content of x is over 0.07. Concurrently, the superconductivity is enhanced monotonically from $T_c \sim 2.8$ K at $x = 0$ to 5.2 K at $x = 0.12$. Intriguingly, in the absence of CDW, $Cs(V_{1-x}Ta_x)_3Sb_5$ ($x = 0.12$) crystals exhibit a pronounced two-fold symmetry of the in-plane angular-dependent magnetoresistance (AMR) in the superconducting state, indicating the anisotropic superconducting properties in the $Cs(V_{1-x}Ta_x)_3Sb_5$. Our findings demonstrate that $Cs(V_{1-x}Ta_x)_3Sb_5$ with the non-trivial band topology is an excellent platform to explore the superconductivity mechanism and intertwined electronic orders in quantum materials.

Keywords: kagome superconductor, charge density wave, rotation symmetry breaking

PACS: 74.25.–q, 71.45.Lr, 11.30.Qc **DOI:** 10.1088/1674-1056/ad4ffa

1. Introduction

Kagome lattice, formed by corner-sharing triangles, naturally hosts special electronic structures including flat bands, Dirac fermions and van Hove singularity (VHS).[1] It provides a fertile platform to explore the magnetism,[2,3] quantum spin liquid,[4] non-trivial topological band[5] and superconductivity.[6] The recently discovered vanadium-based kagome superconductor family AV_3Sb_5 (A = K, Rb, Cs) has attracted tremendous attention. The material family showcases the non-trivial Z_2 band topology,[7] CDW (78 K–105 K),[8] superconductivity (0.8 K–3 K),[6,9,10] nematicity[11] and chiral charge order.[12] For interesting CDW states, the $2a_0 \times 2a_0$ charge modulation exhibits a chiral anisotropy with an unusual magnetic field response.[13] Chiral flux phases and orbital currents are proposed to explain the unconventional CDW, which can give rise to the broken time-reversal symmetry and anomalous Hall effect.[14–17] The three-dimensional properties of CDW are also observed although the stacking patterns ($2a_0 \times 2a_0 \times 2a_0$ or $2a_0 \times 2a_0 \times 4a_0$) remain controversial. For the intriguing superconducting states, double-dome superconductivity under pressure[18–20] is observed and ascribed to a possible stripe-like CDW order.[21] A finite residual linear term of thermal conductivity in zero magnetic field and its large field dependence give evidence for nodal superconducting gap.[22] A clear exponential behavior in magnetic penetration depth suggests a nodeless superconductivity.[23] Specially, the pair density wave with unconventional superconductivity[24] and possible higher-charge superconductivity[25,26] are observed in CsV_3Sb_5. These results indicate that the full comprehensive understanding of superconductivity mechanism still requires further studies.

Spontaneous rotation symmetry breaking (RSB) in the superconducting state is an important phenomenon that sheds light on the underlying superconductivity mechanism.[27,28] In our previous work, a two-fold symmetry of in-plane angular magnetoresistance (AMR) in CsV_3Sb_5 was observed in the mixed state,[29] which indicates the anisotropic superconducting properties. Due to the intertwining of CDW, nematicity and topological superconductivity, the mechanism of two-fold AMR in the superconducting state is difficult to determine.[30] Chemical doping can provide an effective way to modulate the superconductivity and other intertwined orders, the enhanced superconductivity with the suppression of CDW and double-dome superconducting characteristic are observed in the chemical doping CsV_3Sb_5, including $CsV_{3-x}Ti_xSb_5$

†These authors contributed equally to this work.
‡Corresponding author. E-mail: htyang@iphy.ac.cn

and $CsV_3Sb_{5-x}Sn_x$.[31,32] Under the inspiration, the Ta-doped CsV_3Sb_5 shows the highest T_c in the AV_3Sb_5 family materials under the ambient pressure, and isotropic nodeless superconducting gap for the insights into the superconducting pairing mechanism.[33] However, the electrical transport study on the symmetry of superconducting states in $Cs(V_{1-x}Ta_x)_3Sb_5$ is still absent.

In this work, we have successfully synthesized Ta-doped $Cs(V_{1-x}Ta_x)_3Sb_5$ ($0 \le x \le 0.12$) single crystals by a modified self-flux method and investigated the evolution of superconductivity and CDW with doping concentration via the electrical transport measurements. With increasing the doping concentration of Ta, the CDW is suppressed gradually and becomes undetectable at the doping concentration over 0.07. Concurrently, superconductivity is enhanced monotonically, indicating a possible competitive relationship between CDW and superconductivity. The upper critical field H_{c2} can be fitted well by using the two-band model in both the pristine CsV_3Sb_5 and $Cs(V_{1-x}Ta_x)_3Sb_5$ crystals, indicating that the multi-band superconducting feature is preserved after the Ta-doing. Interestingly, even in the absence of CDW-induced rotation symmetry breaking, an explicit two-fold symmetry of AMR in the superconducting state can be observed in the $Cs(V_{1-x}Ta_x)_3Sb_5$ ($x = 0.12$) crystal, indicating the existence of pronounced anisotropic superconducting properties. These results suggest that the charge order is not the main reason for the existence of the RSB in Ta-doped CsV_3Sb_5 superconductors. Our work demonstrates that $Cs(V_{1-x}Ta_x)_3Sb_5$ can serve as a new and "clean" platform to explore anisotropic superconducting properties, and furthermore provides new insights into the understanding of topological superconductivity.

2. Preparation of Ta-doped CsV_3Sb_5 crystals

$Cs(V_{1-x}Ta_x)_3Sb_5$ single crystals were synthesized from Cs liquid (Alfa, purity 99.98%), V powder (Alfa, purity 99.9%), Ta powder (Alfa, purity 99.98%) and Sb shot (Alfa, purity 99.999%) via a self-flux method. The mixture of all raw materials was placed into an alumina crucible and then sealed in a quartz ampoule under a high vacuum atmosphere. Subsequently, the sealed quartz ampoule was heated to 1100 °C, held for 72 hours, and gradually cooled down to 500 °C at a rate of 2 °C per hour. Finally, the single crystals were separated from the flux. Due to the high reactivity of the cesium, all preparation procedures were carried out in an argon-filled glovebox, except for the sealing and reaction procedures.

3. Results and discussion

Upon the Ta-doping, Ta atoms would substitute the V atoms in the kagome plane, which results in a stacking structure of Cs–Sb2–(V/Ta)Sb1–Sb2–Cs layers in $Cs(V_{1-x}Ta_x)_3Sb_5$ (as illustrated in Fig. 1(a)).[34] To ensure the Ta doping, a longer duration time and higher incubation temperature were applied in the preparation of $Cs(V_{1-x}Ta_x)_3Sb_5$ single crystals. The as-prepared $Cs(V_{1-x}Ta_x)_3Sb_5$ crystal shows a regular hexagonal morphology (Fig. 1(b)), indicating the perfect growth of the kagome plane with hexagonal symmetry. To determine the doping concentration of Ta, energy dispersive spectroscopy (EDS) was employed. As shown in Fig. 1(c), the peaks of Ta, Cs, V, Sb can be clearly observed at around 1 keV–5 keV, indicating the successful synthesis of Ta-doped CsV_3Sb_5 single crystals. The typical EDS result indicates the atomic ratio of 0.96:2.65:0.35:4.77 for Cs:V:Ta:Sb, corresponding to $x = 0.12$.

As the elements are in the same group, tantalum ions ($r(Ta^{4+}) = 0.68$ Å) have a larger ionic radius than that of vanadium ions ($r(V^{4+}) = 0.58$ Å). The substitution of Ta ions to V ions can induce changes of the crystalline lattice parameters. A series of x-ray diffraction (XRD) patterns at $x = 0$, 0.03, 0.07, 0.09, 0.12 show diffraction peaks of a preferred [00l] orientation (as shown in Fig. 1(d)). The enlarged (004) peak at 38.5° to 38.9° from $K_{\alpha1} = 1.54056$ Å and $K_{\alpha2} = 1.54439$ Å clearly shows a shift to higher degree with the increasing doping concentration (Fig. 1(e)). The lattice parameters a, b, and c are determined to be 5.532 Å, 5,532 Å, and 9.320 Å by the four-circle single crystal diffractometer, which are slightly bigger in a and b axes than those of pristine CsV_3Sb_5 (5.509 Å, 5.509 Å, and 9.340 Å, respectively) due to the larger ionic radius of Ta^{4+}. The tiny lattice change is only 0.4% and 0.2% in a and c axis, indicating a negligible chemical pressure. The x-ray rocking curve analysis reveals that the full width at half maximum (FWHM) of (004) reflection is only 0.12°, suggesting that the crystal is of high quality.

To investigate the evolution of CDW and superconductivity with the increasing doping concentration, the normalized temperature-dependent resistivity curves (ρ–T) were measured with the temperature ranging from 2 K to 300 K and displayed a metallic behavior above 6 K as shown in Fig. 2(a). The anomaly below 94 K indicating the CDW transition was clearly observed in the Ta-doped samples with the low doping concentration and the anomaly was gradually moved to lower temperature as the doping concentration x increased. To more clearly visualize the CDW transition, the derivative electrical resistivity $\mathrm{d}\rho/\mathrm{d}T$ curves are presented in Fig. 2(b). The peaks marked by arrows show the transition temperature T_{CDW}, which decreases from 94 K in pristine sample to about 44 K at $x = 0.07$, and becomes undetectable as x exceeds 0.07. The evolution of superconductivity is opposite to that of CDW. An enlarged view of ρ–T curves below 10 K clearly shows a monotonic increase of the transition temperature of superconductivity T_c with the increase of the doping concentration (Fig. 2(c)). With the increasing doping concentration, T_c increases from 2.8 K at $x = 0$ to about 4.0 K at $x = 0.07$, and eventually to approximately 5.2 K at $x = 0.12$. The phase diagram of $Cs(V_{1-x}Ta_x)_3Sb_5$ single crystals is presented in Fig. 2(d), where T_{CDW} and T_c are summarized as a function of substitution content x. It can be found that the superconductivity is monotonically enhanced upon the suppression of CDW, which is distinct from the emergence of double-dome in the pressed CsV_3Sb_5 and $CsV_{3-x}Ti_xSb_5$. In the $Cs(V_{1-x}Ta_x)_3Sb_5$ case, the boosting superconductivity can contribute to the rare coexistence of both electrons and holes at the VHS, which induces an attractive component of the Coulomb interaction for an unconventional electronic pairing.[35]

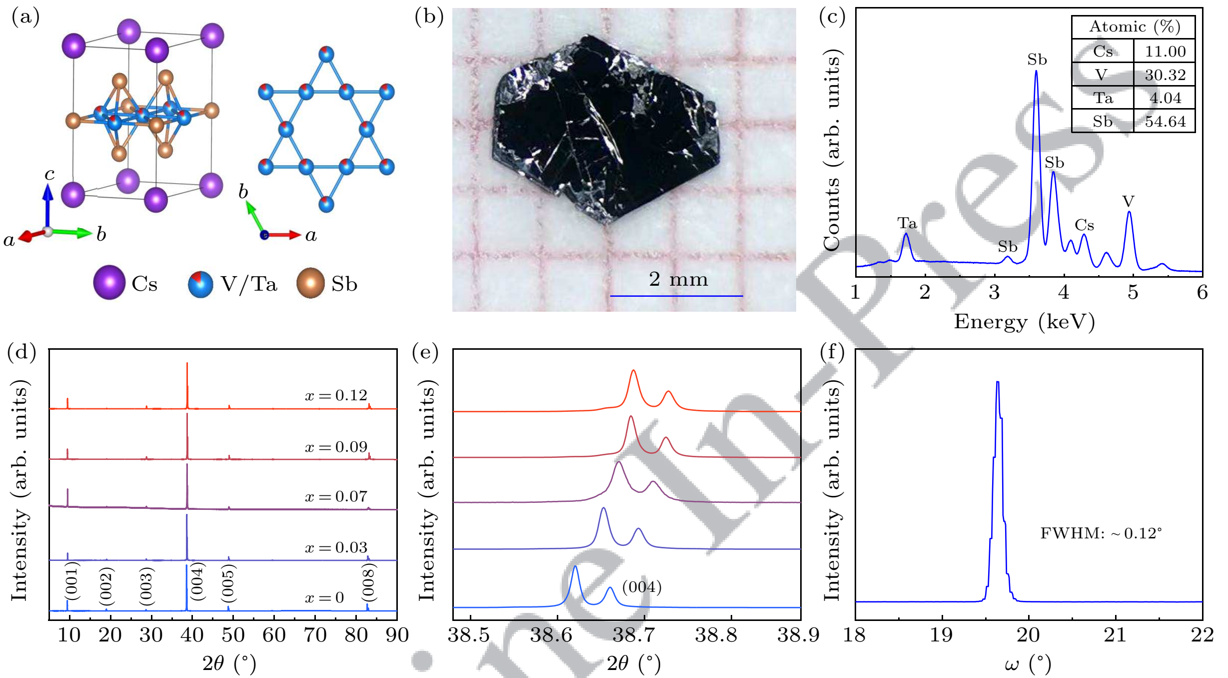

Fig. 1. Characterization of $Cs(V_{1-x}Ta_x)_3Sb_5$. (a) Schematic diagram of crystal structure of Ta-substituted $Cs(V_{1-x}Ta_x)_3Sb_5$. The Cs atoms are depicted in blue, Sb atoms in yellow, V atoms in green and Ta atoms in red. The V atoms form a perfect kagome layer and are replaced by Ta atoms partially. (b) An optical photograph of a $Cs(V_{1-x}Ta_x)_3Sb_5$ crystal, showing hexagonal morphology. (c) Energy dispersion spectrum of a typical sample, indicating an atomic ratio of Cs:V:Ta:Sb = 11.00:30.32:4.04:54.64. (d) XRD patterns of a series of $Cs(V_{1-x}Ta_x)_3Sb_5$ single crystals, showing the same reflections. (e) A detailed view of the XRD pattern around 38.7° shows the (004) peak shifting to higher degrees as the doping concentration increases, indicating a slight change in the c-axis parameter due to the Ta substitution. (f) The rocking curve of (004) reflection, showing a small FWHM of 0.12°.

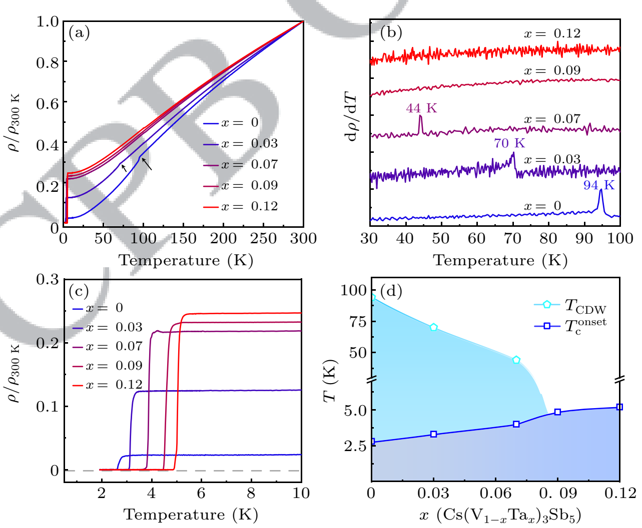

Fig. 2. Electrical transport properties of $Cs(V_{1-x}Ta_x)_3Sb_5$. (a) The normalized temperature-dependent resistivity ρ–T curves at 2 K–300 K. (b) The derivative of electrical resistivity ($d\rho/dT$) curves, indicating the evolution of the CDW transitions at low doping concentrations. (c) An enlarged view below 10 K of (a), showing an enhanced superconductivity upon the Ta-doping. (d) Phase diagram of $Cs(V_{1-x}Ta_x)_3Sb_5$ with the increasing doping concentrations.

To obtain the superconducting upper critical field $H_{c2}(T)$ for both the pristine CsV_3Sb_5 and $Cs(V_{1-x}Ta_x)_3Sb_5$ ($x = 0.12$) crystals, the normalized temperature-dependent resistivity ρ–T under different magnetic fields were conducted. As shown in Figs. 3(a) and 3(b), the resistivity transitions show no significant broadening in out-of-plane magnetic fields. The temperature-dependent upper critical fields are plotted in Fig. 3(c), where $H_{c2}(T)$ corresponds to 50% of the normal state resistance. The temperature dependence of the obtained out-of-plane H_{c2} shows positive curvatures near T_c. Accordingly, the behavior of H_{c2} is well fitted by a two-band model and the zero-temperature critical field $H_{c2}(0)$ is estimated at 0.26 T for $x = 0$ and 1.7 T for $x = 0.12$,[36] indicating a seven times enhancement. The similar enhancement is observed in the in-plane critical field, as shown in Figs. 3(d) and 3(e), the $H_{c2}(0)$ also increases from 2.7 T for $x = 0$ T to 7.6 T for $x = 0.12$. These results demonstrate that Ta-doping significantly enhances not only T_c, but also the critical field. The coherence lengths can be derived from the upper critical fields via

$\mu_0 H_{c2,c} = \Phi_0/(2\pi\xi_c^2)$ and $\mu_0 H_{c2,ab} = \Phi_0/(2\pi\xi_{ab}\xi_c)$. Here, the Φ_0 is the magnetic flux quantum. The derived data are summarized in Table 1. The anisotropic ratio of the coherence length for the sample with $x = 0.12$ is $\gamma = \xi_{ab}/\xi_c \approx 4$, which is smaller than $\gamma \approx 9$ for the pristine CsV_3Sb_5. Since the angle-resolved photoemission spectroscopy results reveal a VHS perfectly aligned with the Fermi level with negligible changes on other low-energy states and their associated electron–boson coupling as a function of the Ta doping, a direct link between the substantially enhanced superconductivity and the VHS at the Fermi level is proposed.[35] Thus, the smaller anisotropic ratio of the coherence length for $Cs(V_{1-x}Ta_x)_3Sb_5$ ($x = 0.12$) crystals can be ascribed to the appearance of the VHS at Fermi level after the Ta doping.

Table 1. Superconducting parameters of pristine and Ta-doped CsV_3Sb_5 crystals.

	T_c (K)	$\mu_0 H_{c2,ab}(0)$ (T)	$\mu_0 H_{c2,c}(0)$ (T)	ξ_c (nm)	ξ_{ab} (nm)	γ
CsV_3Sb_5	2.8	2.7	0.26	3.43	35.58	10
$Cs(V_{1-x}Ta_x)_3Sb_5$ ($x = 0.12$)	5.2	7.6	1.7	3.11	13.91	4

In the pristine CsV_3Sb_5, a two-fold symmetry of resistance in the mixed state has been observed in our previous work.[29,30] To further investigate the anisotropic superconductivity in $Cs(V_{1-x}Ta_x)_3Sb_5$, we conducted the AMR measurements of $Cs(V_{1-x}Ta_x)_3Sb_5$ ($x = 0.12$) crystal since it can provide a relatively "clean" platform without the interference of CDW to explore the symmetry of the superconducting state. The in-plane AMR was measured below T_c of 5.0 K with magnetic field rotating within the ab-plane ($H \| ab$). Figure 4(a) presents the AMR results at 4.5 K under an in-plane magnetic field from 0 T to 5 T. Since the resistivity minimum touches zero in the AMR curve measured at 0.1 T, the two-fold symmetry of AMR curves is supposed to be induced by the anisotropic properties of the superconducting state. The AMR curves under 0.5 T and 0.7 T exhibit a pronounced two-fold symmetry, showing two minima near $\theta = 75^\circ$ and 255° in the absence of CDW. To estimate the strength of relative change of the anisotropic AMR signal, the ratios of $\left(\frac{\Delta R}{R_{min}} = \frac{(R(\theta,T)-R_{min}(T))}{R_{min}(T)} \times 100\%\right)$ are summarized in Fig. 4(b) by polar-coordinate plots. The AMR ratio reaches up to 110% at 0.5 T, which reveals the emergence of strong anisotropic scatterings under the magnetic field in the mixed state. Such a high AMR ratio also indicates that the anisotropic magnetoresistance is not dominated by the minor misalignment angles between the magnetic field and the ab plane. With the increasing magnetic fields above 1.5 T, AMR curves are dominated by normal-state properties. Surprisingly, the two-fold symmetry of $Cs(V_{1-x}Ta_x)_3Sb_5$ crystal disappears at 4.5 K under 2 T and 5 T, which indicates the absence of RSB in the normal state.

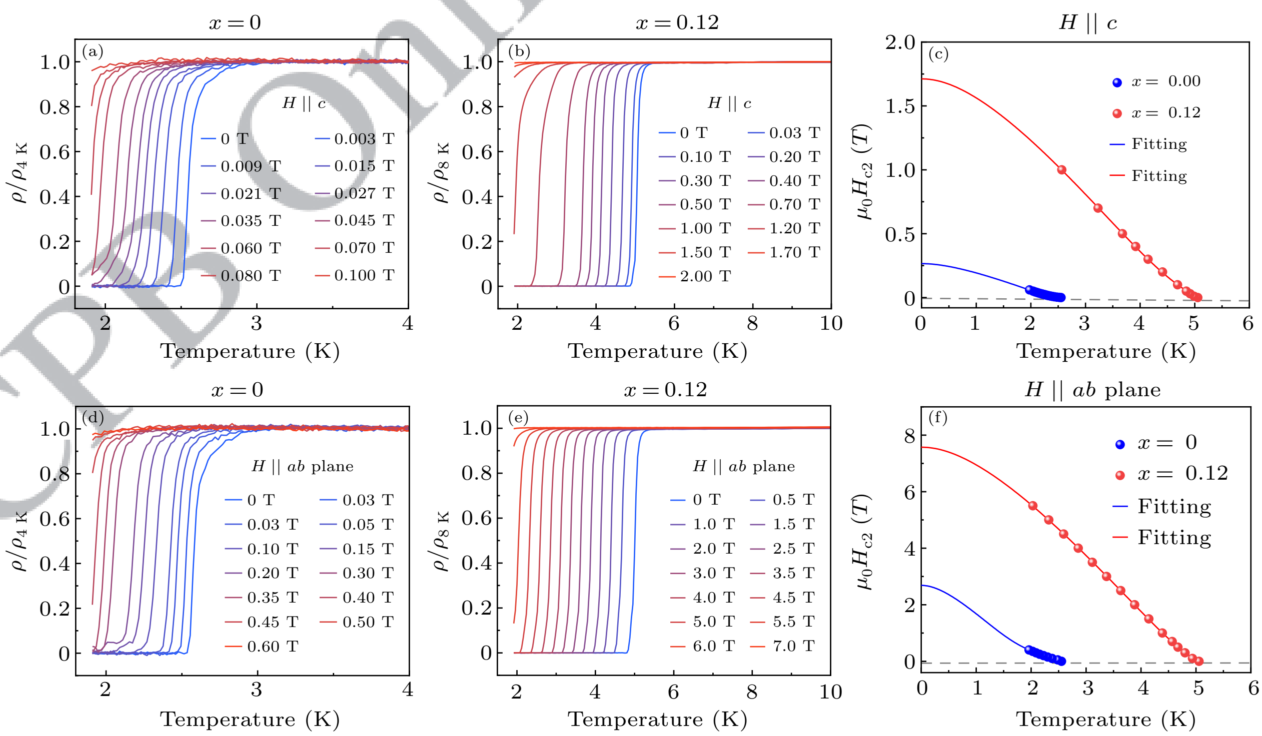

Fig. 3. The ρ–T curves of the pristine CsV_3Sb_5 and $Cs(V_{1-x}Ta_x)_3Sb_5$ ($x = 0.12$) crystals under different magnetic fields. (a) and (b) The normalized ρ–T curves of the pristine CsV_3Sb_5 (a) and $Cs(V_{1-x}Ta_x)_3Sb_5$ ($x = 0.12$) (b) under the applied fields parallel to the c axis. (c) The superconducting critical temperature (T_c) and the upper critical field (H_{c2}) obtained from the $R(T)$ data in (a) and (b) at 50% of the normal state value. (d) and (e) The normalized ρ–T curves with the applied fields parallel to the ab plane in the pristine CsV_3Sb_5 (d) and $Cs(V_{1-x}Ta_x)_3Sb_5$ ($x = 0.12$) (e). (f) The extracted T_c and H_{c2} from (d) and (e).

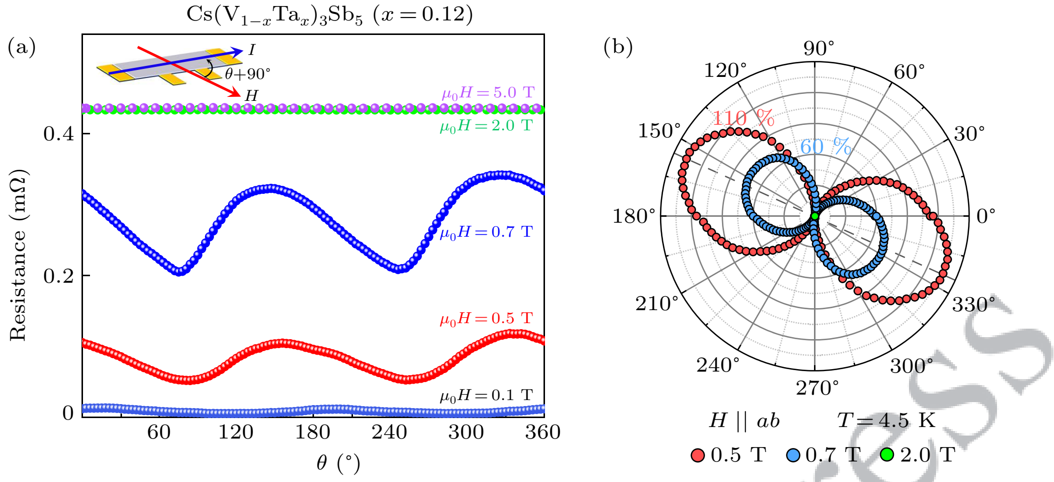

Fig. 4. Anisotropic superconducting states in Cs(V$_{1-x}$Ta$_x$)$_3$Sb$_5$ ($x = 0.12$). (a) The in-plane angular magnetoresistance (AMR) of Cs(V$_{1-x}$Ta$_x$)$_3$Sb$_5$ ($x = 0.12$) at $T = 4.5$ K. A pronounced two-fold symmetry of the in-plane resistance is observed at $\mu_0 H = 0.5$ T and 0.7 T. Here, θ is defined as the angle between the direction of the applied magnetic field and the current, with $\theta = 0°$ corresponding to $H \perp I$, as illustrated in the schematic diagram. (b) AMR ratio $[\Delta R/R_{\min} = (R(\theta,T) - R_{\min}(T))/R_{\min}(T) \times 100\%]$ in the polar coordinate, showing a large AMR ratio of approximately 110% at $\mu_0 H = 0.5$ T.

Based on the above results, the effect of CDW can be excluded since a pronounced two-fold symmetry of resistivity still exists in the superconducting state of the Cs(V$_{1-x}$Ta$_x$)$_3$Sb$_5$ ($x = 0.12$) in the absence of CDW. And the two-fold symmetry is also impossible from the nematicity since it becomes undetectable in the normal state.[35] Generally, the superconductivity accompanied by RSB is a common feature in topological superconductors, such as Cu$_x$Bi$_2$Se$_3$ and Sr$_x$Bi$_2$Se$_3$.[37–39] In a topological superconductor, the unconventional superconductivity with the odd-parity pairing symmetry will exhibit an anisotropic response as the field rotates within the plane.[37] CsV$_3$Sb$_5$ is proposed to be a topological superconductor,[6,40,41] suggesting that the observed RSB may be attributable to the odd-parity pairing symmetry of the superconducting electrons. Additionally, a recent μSR measurement on the CDW-suppressed Cs(V$_{1-x}$Ta$_x$)$_3$Sb$_5$ ($x = 0.14$) sample is mentioned to provide evidence for the potential presence of time-reversal symmetry-breaking superconductivity, which suggests the complex superconductivity in the AV$_3$Sb$_5$ family materials.[33] Further investigation is desired to understand the origin and this symmetry feature of the anisotropic superconducting properties in both pristine and Ta-doped samples.

4. Conclusion

We have successfully synthesized a series of Ta-doped CsV$_3$Sb$_5$ samples with different Ta doping concentrations using a modified self-flux method. Electric transport measurements reveal that superconductivity is monotonically enhanced from T_c of 2.8 K for $x = 0$ to 5.2 K for $x = 0.12$ by the Ta-doping. While, the CDW transition is suppressed rapidly and becomes undetectable with the Ta doping concentration over 0.07. The Cs(V$_{1-x}$Ta$_x$)$_3$Sb$_5$ ($x > 0.07$) with the absence of CDW provides a clean platform to investigate the intrinsic superconductivity. The in-plane AMR of Cs(V$_{1-x}$Ta$_x$)$_3$Sb$_5$ ($x = 0.12$) shows a pronounced two-fold symmetry in the superconducting state with an enhanced superconductivity. This work reveals that the anisotropic superconducting property is still preserved in the Ta-doped CsV$_3$Sb$_5$ without CDW, indicating the robustness of the RSB in the superconducting state.

Acknowledgments

Project supported by the National Key R&D Program of China (Grant No. 2022YFA1204100), the National Natural Science Foundation of China (Grant No. 62488201), the Chinese Academy of Sciences (Grant Nos. XDB33030000, ZDBS-SSW-WHC001, YSBR-003, and YSBR-053), and Innovation Program of Quantum Science and Technology (Grant No. 2021ZD0302700).

References

[1] Wang W S, Li Z Z, Xiang Y Y and Wang Q H 2013 *Phys. Rev. B* **87** 115135
[2] Morali N, Batabyal R, Nag P K, Liu E, Xu Q, Sun Y, Yan B, Felser C, Avraham N and Beidenkopf H 2019 *Science* **365** 1286
[3] Yin J X, Ma W, Cochran T A, Xu X, Zhang S S, Tien H J, Shumiya N, Cheng G, Jiang K, Lian B, Song Z, Chang G, Belopolski I, Multer D, Litskevich M, Cheng Z J, Yang X P, Swidler B, Zhou H, Lin H, Neupert T, Wang Z, Yao N, Chang T R, Jia S and Zahid Hasan M 2020 *Nature* **583** 533
[4] Khuntia P, Velazquez M, Barthélemy Q, Bert F, Kermarrec E, Legros A, Bernu B, Messio L, Zorko A and Mendels P 2020 *Nat. Phys.* **16** 469
[5] Kiesel M L, Platt C and Thomale R 2013 *Phys. Rev. Lett.* **110** 126405
[6] Ortiz B R, Teicher S M L, Hu Y, Zuo J L, Sarte P M, Schueller E C, Abeykoon A M M, Krogstad M J, Rosenkranz S, Osborn R, Seshadri R, Balents L, He J and Wilson S D 2020 *Phys. Rev. Lett.* **125** 247002
[7] Hu Y, Teicher S M L, Ortiz B R, Luo Y, Peng S, Huai L, Ma J, Plumb N C, Wilson S D, He J and Shi M 2022 *Sci. Bull.* **67** 495
[8] Zhao H, Li H, Ortiz B R, Teicher S M L, Park T, Ye M, Wang Z, Balents L, Wilson S D and Zeljkovic I 2021 *Nature* **599** 216

[9] Ortiz B R, Sarte P M, Kenney E M, Graf M J, Teicher S M L, Seshadri R and Wilson S D 2021 *Phys. Rev. Mater.* **5** 034801

[10] Yin Q, Tu Z, Gong C, Fu Y, Yan S and Lei H 2021 *Chin. Phys. Lett.* **38** 037403

[11] Nie L, Sun K, Ma W, Song D, Zheng L, Liang Z, Wu P, Yu F, Li J, Shan M, Zhao D, Li S, Kang B, Wu Z, Zhou Y, Liu K, Xiang Z, Ying J, Wang Z, Wu T and Chen X 2022 *Nature* **604** 59

[12] Guo C, Putzke C, Konyzheva S, Huang X, Gutierrez-Amigo M, Errea I, Chen D, Vergniory M G, Felser C, Fischer M H, Neupert T and Moll P J W 2022 *Nature* **611** 461

[13] Jiang Y X, Yin J X, Denner M M, Shumiya N, Ortiz B R, Xu G, Guguchia Z, He J, Hossain M S, Liu X, Ruff J, Kautzsch L, Zhang S S, Chang G, Belopolski I, Zhang Q, Cochran T A, Multer D, Litskevich M, Cheng Z J, Yang X P, Wang Z, Thomale R, Neupert T, Wilson S D and Hasan M Z 2021 *Nat. Mater.* **20** 1353

[14] Yang S Y, Wang Y, Ortiz B R, Liu D, Gayles J, Derunova E, Gonzalez-Hernandez R, Šmejkal L, Chen Y, Parkin S S P, Wilson S D, Toberer E S, McQueen T and Ali M N 2020 *Sci. Adv.* **6** eabb6003

[15] Feng X, Jiang K, Wang Z and Hu J 2021 *Sci. Bull.* **66** 1384

[16] Denner M M, Thomale R and Neupert T 2021 *Phys. Rev. Lett.* **127** 217601

[17] Mielke C, Das D, Yin J X, Liu H, Gupta R, Jiang Y X, Medarde M, Wu X, Lei H C, Chang J, Dai P, Si Q, Miao H, Thomale R, Neupert T, Shi Y, Khasanov R, Hasan M Z, Luetkens H and Guguchia Z 2022 *Nature* **602** 245

[18] Zhang Z, Chen Z, Zhou Y, Yuan Y, Wang S, Wang J, Yang H, An C, Zhang L, Zhu X, Zhou Y, Chen X, Zhou J and Yang Z 2021 *Phys. Rev. B* **103** 224513

[19] Yu F H, Ma D H, Zhuo W Z, Liu S Q, Wen X K, Lei B, Ying J J and Chen X H 2021 *Nat. Commun.* **12** 3645

[20] Chen K Y, Wang N N, Yin Q W, Gu Y H, Jiang K, Tu Z J, Gong C S, Uwatoko Y, Sun J P, Lei H C, Hu J P and Cheng J G 2021 *Phys. Rev. Lett.* **126** 247001

[21] Zheng L, Wu Z, Yang Y, Nie L, Shan M, Sun K, Song D, Yu F, Li J, Zhao D, Li S, Kang B, Zhou Y, Liu K, Xiang Z, Ying J, Wang Z, Wu T and Chen X 2022 *Nature* **611** 682

[22] Zhao C C, Wang L S, Xia W, Yin Q W, Ni J M, Huang Y Y, Tu C P, Tao Z C, Tu Z J, Gong C S, Lei H C, Guo Y F, Yang X F and Li S Y 2021 arXiv:2102.08356 [cond-mat.supr-con]

[23] Duan W, Nie Z, Luo S, Yu F, Ortiz B R, Yin L, Su H, Du F, Wang A, Chen Y, Lu X, Ying J, Wilson S D, Chen X, Song Y and Yuan H 2021 *Sci. China Phys. Mech. Astron.* **64** 107462)

[24] Chen H, Yang H, Hu B, Zhao Z, Yuan J, Xing Y, Qian G, Huang Z, Li G, Ye Y, Ma S, Ni S, Zhang H, Yin Q, Gong C, Tu Z, Lei H, Tan H, Zhou S, Shen C, Dong X, Yan B, Wang Z and Gao H J 2021 *Nature* **599** 222

[25] Zhou S and Wang Z 2022 *Nat. Commun.* **13** 7288

[26] Ge J, Wang P, Xing Y, Yin Q, Wang A, Shen J, Lei H, Wang Z and Wang J 2024 *Phys. Rev. X* **14** 021025

[27] Wu J, Bollinger A T, He X and Božović I 2017 *Nature* **547** 432

[28] Ji H, Liu Y, Li Y, Ding X, Xie Z, Ji C, Qi S, Gao X, Xu M, Gao P, Qiao L, Yang Y feng, Zhang G M and Wang J 2023 *Nat. Commun.* **14** 7155

[29] Ni S, Ma S, Zhang Y, Yuan J, Yang H, Lu Z, Wang N, Sun J, Zhao Z, Li D, Liu S, Zhang H, Chen H, Jin K, Cheng J, Yu L, Zhou F, Dong X, Hu J, Gao H J and Zhao Z 2021 *Chin. Phys. Lett.* **38** 057403

[30] Ying Xiang, Li Q, Li Y, Xie W, Yang H, Wang Z, Yao Y and Wen H H 2021 *Nat. Commun.* **12** 6727

[31] Yang H, Huang Z, Zhang Y, Zhao Z, Shi J, Luo H, Zhao L, Qian G, Tan H, Hu B, Zhu K, Lu Z, Zhang H, Sun J, Cheng J, Shen C, Lin X, Yan B, Zhou X, Wang Z, Pennycook S J, Chen H, Dong X, Zhou W and Gao H J 2022 *Sci. Bull.* **67** 2176

[32] Oey Y M, Ortiz B R, Kaboudvand F, Frassineti J, Garcia E, Cong R, Sanna S, Mitrović V F, Seshadri R and Wilson S D 2022 *Phys. Rev. Mater.* **6** L041801

[33] Zhong Y, Liu J, Wu X, Guguchia Z, Yin J X, Mine A, Li Y, Najafzadeh S, Das D, Mielke C, Khasanov R, Luetkens H, Suzuki T, Liu K, Han X, Kondo T, Hu J, Shin S, Wang Z, Shi X, Yao Y and Okazaki K 2023 *Nature* **617** 488

[34] Liu J, Li Q, Li Y, Fan X, Li J, Zhu P, Deng H, Yin J X, Yang H, Li J, Wen H H and Wang Z 2024 *Sci. Rep.* **14** 9580

[35] Luo Y, Han Y, Liu J, Chen H, Huang Z, Huai L, Li H, Wang B, Shen J, Ding S, Li Z, Peng S, Wei Z, Miao Y, Sun X, Ou Z, Xiang Z, Hashimoto M, Lu D, Yao Y, Yang H, Chen X, Gao H J, Qiao Z, Wang Z and He J 2023 *Nat. Commun.* **14** 3819

[36] Gurevich A 2003 *Phys. Rev. B* **67** 184515

[37] Sato M and Ando Y 2017 *Rep. Prog. Phys.* **80** 076501

[38] Matano K, Kriener M, Segawa K, Ando Y and Zheng G Q 2016 *Nat. Phys.* **12** 852

[39] Asaba T, Lawson B J, Tinsman C, Chen L, Corbae P, Li G, Qiu Y, Hor Y S, Fu L and Li L 2017 *Phys. Rev. X* **7** 011009

[40] Liang Z, Hou X, Zhang F, Ma W, Wu P, Zhang Z, Yu F, Ying J J, Jiang K, Shan L, Wang Z and Chen X H 2021 *Phys. Rev. X* **11** 031026

[41] Fu Y, Zhao N, Chen Z, Yin Q, Tu Z, Gong C, Xi C, Zhu X, Sun Y, Liu K and Lei H 2021 *Phys. Rev. Lett.* **127** 207002